

---

# Hardware Design and Testing for Optical Brain Imaging and Visible Light Communication

Md Nabil Shehtab Dhrubo

Electrical, Computer and Systems Engineering, Rensselaer Polytechnic Institute, Troy, NY 12180

**Abstract**—Miniaturization of spectroscopic tools offers portable solution for several biomedical applications. This report overviews an on-chip functional near infra-red spectroscopy (fNIRS) hardware for optical brain imaging, which offers portable and non-invasive solution for monitoring blood oxygenation level in neural tissues. It mostly discusses receiver front-end of the fNIRS system, which includes a Silicon Avalanche Photodiode (SiAPD), Quench-Reset Circuit for controlling abrupt generation of photocurrent and a Transimpedance Amplifier (TIA) for conversion and amplification of generated photocurrent. Prospective architecture of these components and their respective performances have been thoroughly focused on. The report also briefly discusses an experimental technique to characterize a photodiode-TIA network consisting of standalone photodiode and TIA chips in presence of visible light, which can provide a performance estimate before integrating them on a single chip.

**Index Terms**—fNIRS, APD, QR Circuits, TIA.

## I. INTRODUCTION

Functional Near Infrared Spectroscopy (fNIRS) is a novel technique capable of measuring oxy- and deoxy-hemoglobin quantities in neural tissues by measuring their absorbance as a function of wavelength between 650 nm and 950 nm [1–3]. NIR light can penetrate biological tissues in the range of 0.5 -3 cm allowing investigation of relatively deep brain tissues. A conventional continuous wave fNIRS system consists of an NIR light source, a photodetector with high gain and low noise, a network of post-amplifiers along with filters and data processing modules to process and store the data in a computing system [4-6]. Miniaturizing such a large system on a single chip has been a challenge for researchers over the decades. The transmitter front end of the system contains an NIR source (usually an LED or a laser diode) that is placed near the scalp. The analog front end of the receiver usually starts with an Avalanche Photodiode (APD) that multiplies generated photocarriers for converting incident optical signal into a continuous electrical signal. For integrating APDs with other CMOS devices on a monolithic platform, researchers have investigated fabrication of Silicon APDs in standard CMOS process [7-8]. APDs can operate in linear mode (amplification mode) or in Geiger mode

(single photon counting mode). When they operate in Geiger mode, they are typically called Single Photon Avalanche Photodiodes (SPADs). Usually, a SPAD operates at a reverse bias higher than breakdown voltage. In order to control the SPAD photocurrent and prevent it from going deep into breakdown, quench-and-reset circuits are designed to absorb large amount of avalanche photocurrent generated during Geiger mode operation [9]. The photocurrent generated from APD is then fed to a Trans-impedance Amplifier (TIA) to convert it into an amplified voltage signal. In order to eliminate residual noise and ensure stability of TIA, the output voltage of TIA is then passed through a limiting amplifier (LA) and filter [10]. Finally, for processing received data and making it machine-readable, the analog voltage pulse is sent through an Analog-to-Digital (ADC) converter. Fig. 1 shows a simplified schematic of an fNIRS system [11]. Such a photodiode-TIA network can also be utilized for Visible Light Communication (VLC) [12]. This report presents a detailed discussion on prospective APD architectures, conventional design of quench-and-reset circuits and TIA architectures along with parameters that determine the suitability of these designs, particularly for biomedical imaging. It also briefly discusses experimental methods and simulation techniques of testing such a network for visible light communication.

## II. APD ARCHITECTURES

Over the years, III-V material based APDs have been widely used for various short- and mid- wavelength Infrared operations and high-speed fiber optics communication [13-16]. However, with recent advancements in Silicon Photonics technology, Silicon based and Ge/Si based APDs have become popular for next generation of LiDAR and biomedical imaging applications due to better compatibility with CMOS foundry [17-19]. Fig. 2 shows two prospective top-illuminated Silicon APD structures suitable for NIR detection [20].

In the first structure, Photons are mostly absorbed at active junction between p+ region and deep n-well. After getting absorbed, energy from a single photon creates an Electron-Hole Pair (EHP), which then gets multiplied via impact ionization mechanism.

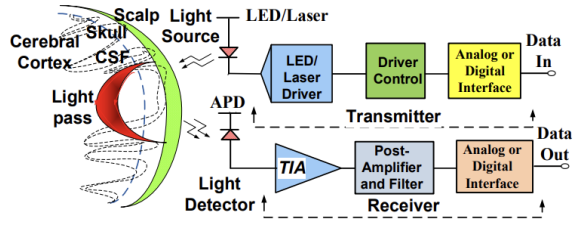
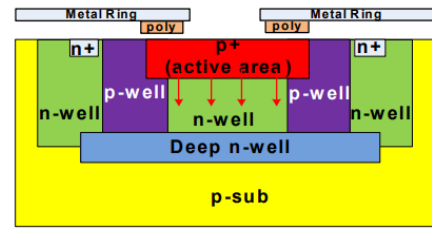


Figure 1. Simplified Schematic of an fNIRS system [11]

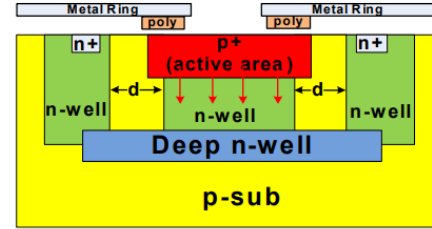
Typically, impact ionization occurs in region where electric field is the highest so that generated EHP can obtain sufficient energy to create more free carriers. Since most depletion region or space charge region is inside n-well between p+ region and deep n-well, electric field is highest inside n-well and multiplication of generated photocarriers occurs in this region as well. After multiplication, electrons drift laterally towards n+ region through p well and holes drift towards p+ region. The p-well regions act as guard rings to prevent premature edge breakdown at the peripheral edges with higher curvature. Fig. 1b shows another photodiode architecture where the active junction exists between deep n-well and p-substrate. Photocarriers generated in this junction travel towards n-well and gets multiplied. For this structure, deep n-well acts as the charge layer between absorption region and the multiplication region to prevent premature edge breakdown. The charge layer serves as an electric field control layer that ensures that electric field intensity in multiplication region is uniform and sufficient to achieve high gain, while simultaneously keeping the field low enough to prevent tunneling of photocarriers through multiplication region [21].

Fig. 3 shows the Photon Detection Probability (PDP) and Sensitivity of the proposed photodetector structures for various incident wavelengths. APD1 has higher PDP since it has larger absorption region. However, APD2 shows higher sensitivity since APD2 has separate absorption and multiplication region, which leads to lower dark current and lower multiplication noise [22-23].

APDs usually operate in reverse bias ( $V_R$ ) mode, typically close to breakdown voltage. They have two modes of operation-(1) Geiger mode, where they operate as a SPAD beyond breakdown voltage ( $V_{BD}$ ) i.e.  $|V_R| > |V_{BD}|$  and detects single photon and (2) Linear mode or Amplification Mode, where they operate below, but close to breakdown voltage i.e.  $|V_R| < |V_{BD}|$ . This requirement for high operating reverse bias is a limitation of APDs, which can be compensated by using PIN photodiodes, but at the cost of lower gain.

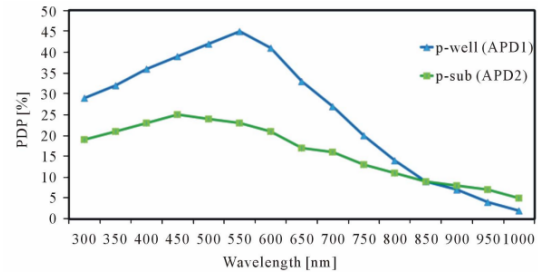


(a)

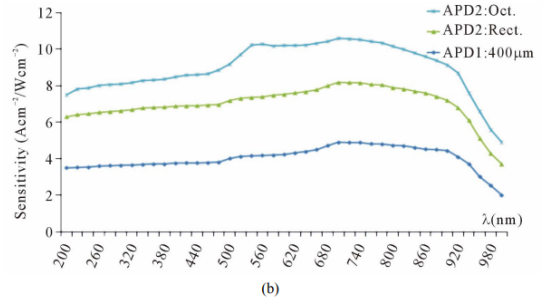


(b)

Figure 2. Two Prospective APD Architectures [20]



(a)



(b)

Figure 3. Performance of Proposed APD Architectures [20]

### III. QUENCH AND RESET CIRCUITS

For Geiger mode operation of APDs, quench and reset (QR) circuit is necessary for interrupting the abruptly generated large avalanche photocurrent and dropping APD bias to normal operating value below breakdown. Once initial photocurrent is quenched, the APD is reset back to bias beyond breakdown for next photon detection. Fig. 4 demonstrates this process [24].

Quench and Reset circuits can be of three types- (1) Passive QR; (2) Active QR and (3) Mixed QR circuits.

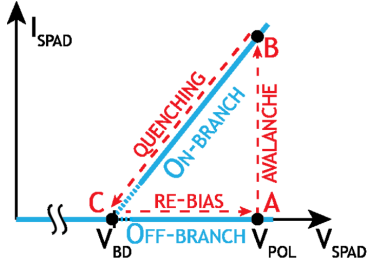


Figure 4. Demonstration of Quench and Reset Operation [24]

Passive QR circuits consist of passive elements such as resistors to absorb avalanche photocurrent. Fig. 5(a) shows two simple passive QR circuits and Fig. 5(b) shows the cathode voltage response upon single photon incidence [20]. Passive QR circuits usually require small area APDs and offer slowest quenching among three configurations. On the contrary, active QR circuits consist of active elements such as transistors to control quench-reset cycle. So, they ensure quicker quenching and can also be integrated to large area APDs. However, active QR circuits are usually quite complex and requires precise design to reduce propagation delay caused by parasitic capacitances of the active elements.

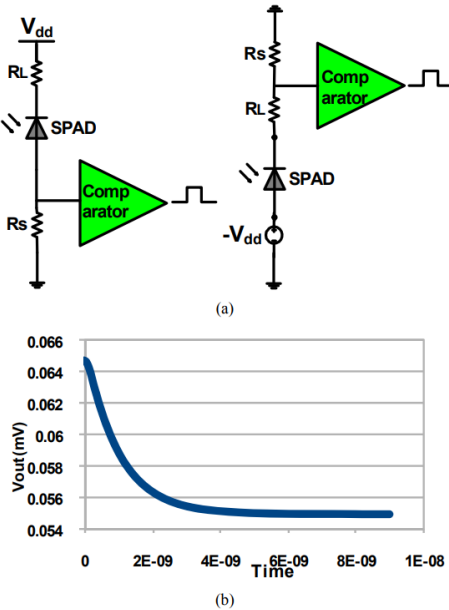


Figure 5. (a) Two Probable Passive QR Networks; (b) Cathode Voltage in Response to Single Photon Incidence [20]

Mixed QR circuits combine passive elements along with active elements; offering reduced complexity than active QR circuits while ensuring faster quenching than passive circuits. Fig. 6 shows such a mixed architecture

[20]. In quiescence condition, when there is no current flowing, the drop through R1 is zero and so cathode terminal of SPAD is biased to Vdd. Consequently, bias across SPAD is above breakdown voltage. Upon photon incidence, SPAD operates in Geiger mode and avalanche current starts to flow through R1, reducing the cathode voltage. When cathode voltage is sufficiently low, it turns ON the Sense transistor  $S_{Sense}$ . As a result, there is a voltage drop through R3 and it turns the quench transistors ( $S_{quench1}$  and  $S_{quench2}$ ) ON via  $S_{feedback}$ . These quench transistors quickly pull the cathode voltage down to ground, bringing bias across SPAD below breakdown. This is how avalanche current is quickly dissipated.

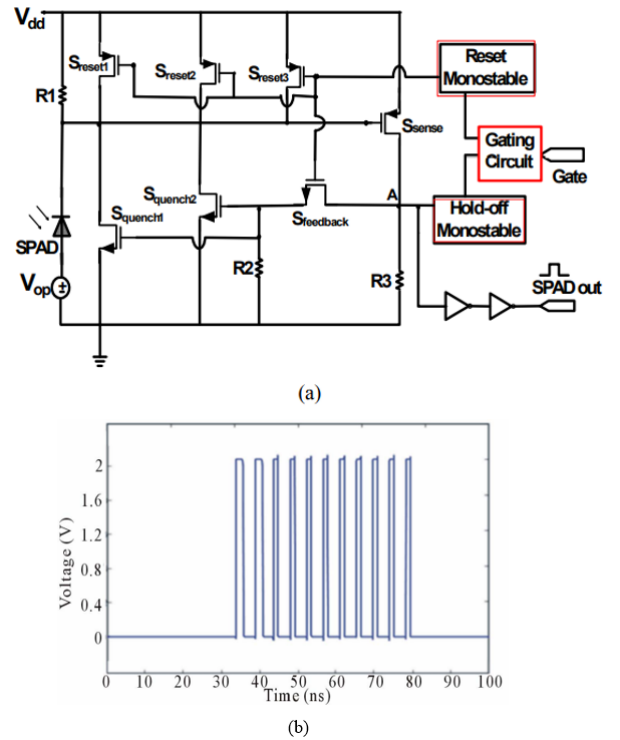


Figure 6. (a) A Mixed QR Circuit (b)APD Cathode Voltage in Response to Multiple Photon Arrivals between 35 and 80 ns [20]

Once hold-off period ends, quench transistors are turned OFF and reset monostable pulse activates the three reset transistors ( $S_{reset1}$ ,  $S_{reset2}$ , and  $S_{reset3}$ ). Since they are connected in parallel configuration, they provide the cathode terminal with a low resistive path to Vdd and consequently, bias across SPAD is reset back to a value higher than breakdown voltage. This makes the SPAD prepared for next photon detection.

#### IV. TIA ARCHITECTURES

The APD terminals are connected to input terminals of a Trans-impedance Amplifier (TIA) in order to convert

the APD photocurrent into an amplified voltage pulse. Three most common topologies of TIA are (1) Common-Gate (CG) TIA; (2) Resistive Feedback (RF) TIA and (3) Capacitive Feedback (CF) TIA [25-30]. Although CG TIA has low input impedance and high transimpedance gain, its input noise is quite high and Bandwidth (BW) is comparatively low. RF TIA offers high gain and shows smallest noise at high frequencies. Also, its BW is large enough for neural signal acquisition (which requires BW of around 100 kHz). CF TIA offers smaller noise at low frequencies but is quite noisy at high frequencies. So, to achieve low input impedance, high transimpedance gain, reasonable BW and low noise during high frequency operation, a combination of CG TIA and RF TIA can be explored. Fig. 7 shows such a combination [20]. Transistors M1, M2 and M4 form a CG TIA while transistors M3, M5 and M8 form RF TIA. Transistors M6, M7 and M9 act as resistive feedback for the RF TIA. The transimpedance gain and Gain-Bandwidth product (GBW) of this mixed TIA configuration are given as:

$$\frac{V_{out}}{I_{in}} = \frac{-g_{m5}R_f - 1}{g_{m4} + g_{m5}} \quad (1)$$

$$GBW = \frac{(g_{m1} + g_{s1})(1 - g_{m5}R_f)}{C_{in} + (g_{m1} + g_{s1})(C_L + C_f)R_f/K_{cm}} \quad (2)$$

where,

$$K_{cm} = \frac{g_{m5}}{g_{m4}} \quad (3)$$

$g_{s1}$  is the body effect transconductance of transistor M1. In order to boost the output voltage swing, the TIA output voltage is passed to an operational transconductance amplifier (OTA) which converts it to a current signal and this current signal is again fed to a TIA for generating a final output voltage having higher swing than the original output from first TIA block. This OTA-TIA combination next to first TIA can also be replaced by a high gain voltage amplifier for circuit simplification. In order to improve stability of the circuit and match output impedance of the second TIA to input impedance of the component following it (usually an ADC), the output voltage from second TIA is passed to a limiting Amplifier (LA). Finally, to remove any residual noise, this limiting amplifier is followed by a filter. Fig. 8 shows the transimpedance gain of overall amplifier network over 1Hz-400MHz frequency range [20].

In equation (2),  $C_{in}$  is the input capacitance of TIA and  $C_f$  is feedback capacitance. Ideal value of  $C_f$  depends on input capacitance  $C_{in}$ , feedback resistance  $R_f$  and unity gain bandwidth  $f_{GBW}$ . Following equation provides the expression for feedback capacitance [12].

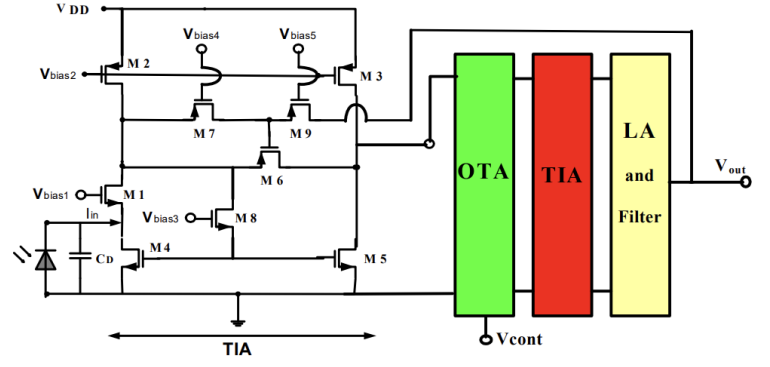


Figure 7. Proposed Combination of CG TIA nad RF TIA [20]

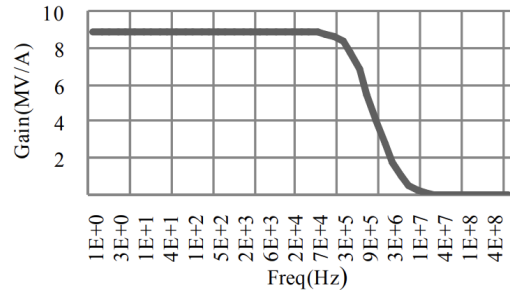


Figure 8. Transimpedance Gain of Proposed TIA Configuration [20]

$$C_f = \sqrt{\frac{C_f + C_{in}}{2\pi R_f f_{GBW}}} \quad (4)$$

This transcendental equation can be solved using iterative method. The 3-dB bandwidth of the TIA depends on terminal capacitance of photodiode  $C_t$  and can be measured using following equation [12].

$$f_{3dB} = \sqrt{\frac{f_{GBW}}{2\pi R_f (C_t + C_{in})}} \quad (5)$$

## V. EXPERIMENTAL SETUP FOR CHARACTERIZATION OF PHOTODIODE-TIA NETWORK IN VISIBLE LIGHT

Fig. 9 shows an experimental setup for characterization of a photodiode-TIA network consisting of standalone APD and TIA chips [12]. This methodology can be used to obtain performance estimate of the combined network before actually integrating APD and TIA on a single chip. The photodiode can be illuminated using an LED and the output optical power of the LED can be modulated using a programmable power supply. The photocurrent and TIA output voltage can be measured using digital multimeter. Reference [12] shows such

an experiment for visible light communication, where researchers swept the power supply from 8V to 14V, with 1A current, so that the LED power can be varied. They used commercially available OPA656 Op-Amp as the TIA and SP8-ML photodiode. The photodiode-TIA circuit is placed at a distance of 50 cm from the LED. Fig. 10 shows experimentally derived dependence of TIA output voltage on LED power for different feedback resistances, which provides an idea of overall photo-conversion efficiency of the Photodiode-TIA network. The Ideal value for feedback capacitance was calculated using equation (4) and ideal value of feedback resistance ( $R_f$ ) can be given as the ratio of output voltage swing to maximum short circuit current.

$$R_f = \frac{V_{out,max} - V_{out,min}}{I_{SC}} \quad (6)$$

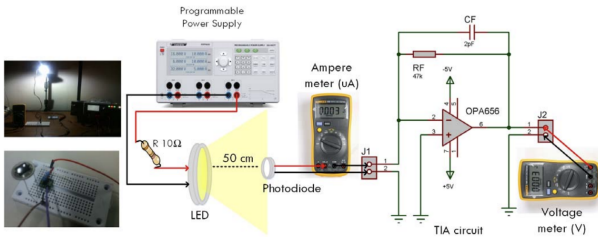


Figure 9. Experimental Setup for Characterization of Photodiode-TIA Network [12]

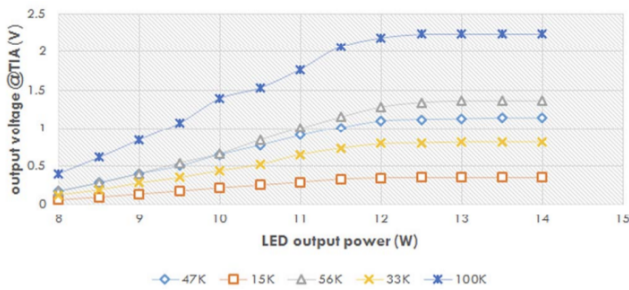
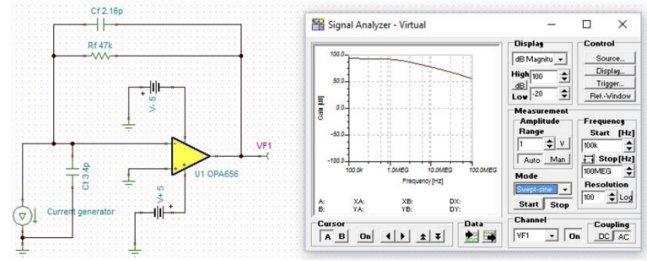
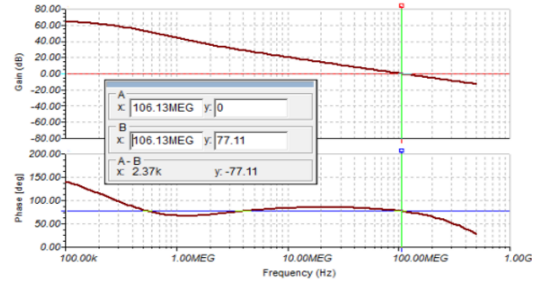


Figure 10. TIA Output Voltage vs LED Output Power [12]

For better validation of experiment, they also compared their experimental results with simulation results. Fig. 11(a) shows simulation setup in Toolkit for Interactive Network Analysis (TINA), a software package from Texas Instruments. Fig. 11(b) shows bode plot of photodiode-TIA network as obtained from simulation. Table 1 shows a comparison of some performance parameters derived from simulation and experiment, which shows enough 3-dB BW for neural signal acquisition and visible light communication.



(a)



(b)

Figure 11. (a) Simulation Setup for Characterization of Photodiode-TIA Network; (b) Bode plot of Overall Photodiode-TIA Network [12]

Table 1  
COMPARISON BETWEEN EXPERIMENTAL AND SIMULATION RESULTS

Parameter	Experimental Result	Simulation Result
$f_{3dB}$	1.5 MHz	1.59 MHz
$V_{out}(0\mu A)$	0.2008 V	0.23245 V
$V_{out}(18\mu A)$	0.9 V	1.08 V

## VI. CONCLUSION

This paper discusses an fNIRS system for optical neural imaging and focuses mostly on researches up to date on receiver front end of the system. For quick photon counting and detection of continuous wave NIR signals, different APD architectures can be explored but fabricating them using CMOS process might be challenging to some extent. Designing precise and small delay QR circuits is very crucial since high delay in QR circuit will cause false re-triggering of avalanche. Designing high SNR APDs and properly integrating them to TIA are significant for reducing input noise of TIA. Since, output noise is considerably high at low frequencies for RF TIAs and high frequencies for CF TIAs, proper filtering circuits are also crucial for appropriate imaging. For integrating this network on a single chip, proper transistor sizing and biasing are important for reducing dynamic power consumption and circuit delays as well as optimizing chip area and improving overall gain.

---

## VII. REFERENCES

- [1] S. R. Arridge, "Optical tomography in medical imaging," *Inverse Problems*, vol. 15, no. 2, p. R41, 1999
- [2] H. Dehghani, B. R. White, B. W. Zeff, A. Tizzard, and J. P. Culver, "Depth sensitivity and image reconstruction analysis of dense imaging arrays for mapping brain function with diffuse optical tomography," *Appl. Opt.*, vol. 48, no. 10, pp. D137–D143, Apr. 2009
- [3] Soren D. Konecky, Amaan Mazhar, David Cuccia, Anthony J. Durkin, John C. Schotland, and Bruce J. Tromberg, "Quantitative optical tomography of sub-surface heterogeneities using spatially modulated structured light," *Opt. Express* 17, 14780-14790 (2009)
- [4] E. Sultan, K. Manseta, A. Khwaja, L. Najafzadeh, A. Gandjbakhche, K. Pourrezaei, and A. S. Daryoush "Modeling and tissue parameter extraction challenges for free space broadband fNIR brain imaging systems", *Proc. SPIE 7902, Imaging, Manipulation, and Analysis of Biomolecules, Cells, and Tissues IX*, 790223 (11 February 2011)
- [5] E. Kamrani, F. Lesage and M. Sawan, "Low-Noise, High-Gain Transimpedance Amplifier Integrated With SiAPD for Low-Intensity Near-Infrared Light Detection," in *IEEE Sensors Journal*, vol. 14, no. 1, pp. 258-269, Jan. 2014
- [6] A. M. Chiarelli et al., "Flexible CW-fNIRS system based on Silicon Photomultipliers: In-vivo characterization of sensorimotor response," 2017 *IEEE SENSORS*, 2017, pp. 1-3
- [7] N. Faramarzpour, M. J. Deen, S. Shirani and Q. Fang, "Fully Integrated Single Photon Avalanche Diode Detector in Standard CMOS 0.18- $\mu\text{m}$  Technology," in *IEEE Transactions on Electron Devices*, vol. 55, no. 3, pp. 760-767, March 2008
- [8] M. Lee, H. Rucker and W. Choi, "Effects of Guard-Ring Structures on the Performance of Silicon Avalanche Photodetectors Fabricated With Standard CMOS Technology," in *IEEE Electron Device Letters*, vol. 33, no. 1, pp. 80-82, Jan. 2012
- [9] I. Berdalović, Ž. Osrečki, F. Šegmanović, D. Grubišić, T. Knežević and T. Suligoj, "Design of passive-quenching active-reset circuit with adjustable hold-off time for single-photon avalanche diodes," 2016 39th International Convention on Information and Communication Technology, Electronics and Microelectronics (MIPRO), 2016, pp. 34-39
- [10] Denisenko, D. Yu et al. "Third-Order Low-Pass Filters for Limiting the Signal Spectrum at the Differential Input of the Analog/Digital Converters" 2020 *J. Phys.: Conf. Ser.* 1443 012011
- [11] E. Kamrani, F. Lesage and M. Sawan, "Low-Noise, High-Gain Transimpedance Amplifier Integrated With SiAPD for Low-Intensity Near-Infrared Light Detection," in *IEEE Sensors Journal*, vol. 14, no. 1, pp. 258-269, Jan. 2014, doi: 10.1109/JSEN.2013.2282624
- [12] S. Fuada, A. P. Putra, Y. Aska and T. Adiono, "Trans-impedance amplifier (HA) design for Visible Light Communication (VLC) using commercially available OP-AMP;" 2016 3rd International Conference on Information Technology, Computer, and Electrical Engineering (ICITACEE), 2016, pp. 31-36
- [13] Li, J., Dehzangi, A., Brown, G. et al. Mid-wavelength infrared avalanche photodetector with AlAsSb/GaSb superlattice. *Sci Rep* 11, 7104 (2021).
- [14] Liang Y, Perumalveeramalai C, Lin G, Su X, Zhang X, Feng S, Xu Y, Li C. A review on III-V compound semiconductor short wave infrared avalanche photodiodes. *Nanotechnology*. 2022 Feb 11. Epub ahead of print. PMID: 35147516.
- [15] M. Nada, F. Nakajima, T. Yoshimatsu, H. Matsuzaki and K. Sano, "High-speed Avalanche Photodiodes based on III-V Compounds for Optical Communications," 2019 *Compound Semiconductor Week (CSW)*, 2019, pp. 1-2
- [16] J. C. Campbell, "Recent Advances in Avalanche Photodiodes," *Journal of Lightwave Technology*, vol. 34, no. 2, pp. 278-285, 15 Jan. 15, 2016
- [17] D. Palubiak, M. M. El-Desouki, O. Marinov, M. J. Deen and Q. Fang, "High-Speed, Single-Photon Avalanche-Photodiode Imager for Biomedical Applications," in *IEEE Sensors Journal*, vol. 11, no. 10, pp. 2401-2412, Oct. 2011
- [18] Cesar Bartolo-Perez, Soroush Chandiparsi, Ahmed S. Mayet, Hilal Cansizoglu, Yang Gao, Wayesh Qarony, Ahasan AhAmed, Shih-Yuan Wang, Simon R. Cherry, M. Saif Islam, and Gerard Ariño-Estrada, "Avalanche photo-detectors with photon trapping structures for biomedical imaging applications," *Opt. Express* 29, 19024-19033 (2021)
- [19] Y. Li, X. Luo, G. Liang, and G. Lo, "Demonstration of Ge/Si Avalanche Photodetector Arrays for Lidar Application," *Optical Fiber Communication Conference (OFC) 2019, OSA Technical Digest (Optica Publishing Group, 2019)*, paper Tu3E.3
- [20] E. Kamrani et al. "Fully On-Chip Integrated Photodetector Front-End Dedicated to Real-Time Portable Optical Brain Imaging." *Optics and Photonics Journal* 02 (2012): 300-313.

---

[21] Junkang Wu et al "Charge layer optimized 4H-SiC SACM avalanche photodiode with low breakdown voltage and high gain" 2019 Jpn. J. Appl. Phys. 58 100913

[22] R. D. Dupuis, J. R. Velebir, J. C. Campbell and G. J. Qua, "Avalanche photodiodes with separate absorption and multiplication regions grown by metalorganic vapor deposition," in IEEE Electron Device Letters, vol. 7, no. 5, pp. 296-298, May 1986, doi: 10.1109/EDL.1986.26379

[23] Hui Wang, Xiaohong Yang, Rui Wang, Tingting He, and Kaibao Liu, "Low dark current and high gain-bandwidth product of avalanche photodiodes: optimization and realization," Opt. Express 28, 16211-16229 (2020)

[24] D. Bronzi, "Front-side and Back-side Illuminated SPAD Arrays for 2D Imaging and 3D Ranging," Politecnico di Milano, 2014

[25] D. C. Dias, F. S. de Melo, L. B. Oliveira and J. P. Oliveira, "Regulated common-gate transimpedance amplifier for radiation detectors and receivers," 2014 Proceedings of the 21st International Conference Mixed Design of Integrated Circuits and Systems (MIXDES), 2014, pp. 540-545

[26] J. Hu, Y. Kim and J. Ayers, "A low power 100M CMOS front-end transimpedance amplifier for biosensing applications," 2010 53rd IEEE International Midwest Symposium on Circuits and Systems, 2010, pp. 541-544

[27] J. -H. Noh, "Frequency-Response Analysis and Design Rules for Capacitive Feedback Transimpedance Amplifier," in IEEE Transactions on Instrumentation and Measurement, vol. 69, no. 12, pp. 9408-9416, Dec. 2020

[28] M. M. R. Ibrahim and P. M. Levine, "CMOS transimpedance amplifier for biosensor signal acquisition," 2014 IEEE International Symposium on Circuits and Systems (ISCAS), 2014, pp. 25-28

[29] Shahdoost, S., Medi, A. Saniei, N. Design of low-noise transimpedance amplifiers with capacitive feedback. Analog Integr Circ Sig Process 86, 233-240 (2016)

[30] V. Balasubramanian, P. -F. Ruedi, Y. Temiz, A. Ferretti, C. Guiducci and C. C. Enz, "A 0.18  $\mu\text{m}$  Biosensor Front-End Based on  $1/f$  Noise, Distortion Cancellation and Chopper Stabilization Techniques," in IEEE Transactions on Biomedical Circuits and Systems, vol. 7, no. 5, pp. 660-673